506. Modeling and diagnostics of gyroscopic rotor

V. Barzdaitis[1,a], M. Bogdevičius[2,b], R. Didžiokas[3,c], M. Vasylius[3,d]

[1]Kaunas University of Technology, Department of Engineering Mechanics, Donelaičio St.73, Kaunas, LT-44244, Lithuania

[2]Vilnius Gediminas Technical University, Department of Transport Technological Equipment, Plytines St. 27 LT-10105, Vilnius, Lithuania

[3]Klaipėda University, Mechatronic Science Institute, Bijūnų St. 17, Klaipėda, LT-91225, Lithuania

E-mail: [a] *vytautas.barzdaitis@ktu.lt,* [b] *marius.bogdevicius@ti.vgtu.lt,* [c] *rimantas.didziokas@ktu.lt,* [d] *marius.vasylius@ku.lt*

Abstract. Study of dynamics of heavy impeller rotor and failure diagnostics of tilting-pad journal bearings is the object of this paper. Induced rubbing process in the bearings at resonance and increased rubbing phenomenon in both bearings was identified experimentally in situ by measuring radial gaps. Rotational speed was established when gravitational force became dominant over rotor gyroscopic force. Rotating system model was designed, simulated and verified.

Keywords: gyroscopic rotor, tilting-pad journal bearings, vibration, diagnostic

Nomenclature

Names	Description	Names	Description
$\{q\}$	The nodal element displacement vector	L_r, L_s, L_μ	Inductive reactance of stator and rotor
$[N]$, $[N_\theta]$	The matrices of shape functions	w_s	Angular velocity of voltage
$\{\dot{\theta}\}$, $\{\omega\}$	Angular velocity	U_{nom}	Voltage
$\{\psi\}$, $\{\dot{\psi}\}$	Flux space vector and time derivative	M_e	Torque of EM
I_e	Inertia mass moment of rotor	pol	Number of EM pole
$\{B_\psi(t,\psi,\dot{\varphi}_e)\}$	Vector of nonlinear functions	$[M(q)]$	Mass matrix
$\left[A_\psi\right]$	Matrix of resistors and inductive reactance of stator and rotor	$[C]$, $[G]$, $[K]$	Damping, gyroscopic, stiffness matrixes
φ_e	Angle of rotor	$\{F(q,\dot{q})\}$	The load vector of the finite element.
$M_e(\psi)$	Electrical torque	F_b, F_{by}, F_{bz}	Fluid-film force components
$M_r(\varphi_i,\dot{\varphi}_i,p_{Gi})$	Resistance torque	$[K_b]$, $[C_b]$	Stiffness, damping matrixes of bearing
r_s, r_r	Resistor of stator and rotor	$\{q_b\}$	Vector of displacement of bearing.

1. Introduction

Stationary condition monitoring, safety and diagnostic systems are mainly applied in the case of critical, expensive machines, and based on vibration and technological parameters measurements [1, 2, 4]. High-efficiency air blower machine is operating in continuous long-term running mode. The machine's induction electric motor journal bearings housings vibration sources were identified and eliminated increasing stiffness of inductor and journal bearings [1]. In this article the condition and failure diagnostics of the radial hydrodynamic tilting-pad journal bearings of the blower rotor is monitored, experimentally tested, modeled and analysis results implemented in industry [5].

2. Condition monitoring and diagnostics of air blower rotor

Air blower machine comprises electric motor EM, double-helical gear multiplier GB increasing rotational speed of the blower rotor BR, Fig. 1. The 5.6 MW power EM rotational speed is 1500 rpm and BR nominal rotational speed is ~3119 rpm.

The technical condition of BR was evaluated by monitoring rotor position in the bearings (gaps) and vibration displacements peak-to-peak values $s_{p-p7,8}$ permanently with four proximity probes fixed at the 7th and 8th bearings and rotational speed with keyphasor transducer SP.

In this article the failure diagnostics of the radial hydrodynamic tilting-pad journal bearings 7th and 8th of the blower rotor BR is monitored, experimentally tested in situ and modeled. The task is to determine the main reasons of failure of tilting-pad journal bearings 7th and 8th and to elaborate recommendations for increasing operation time of the bearings avoiding damages (Fig. 2).
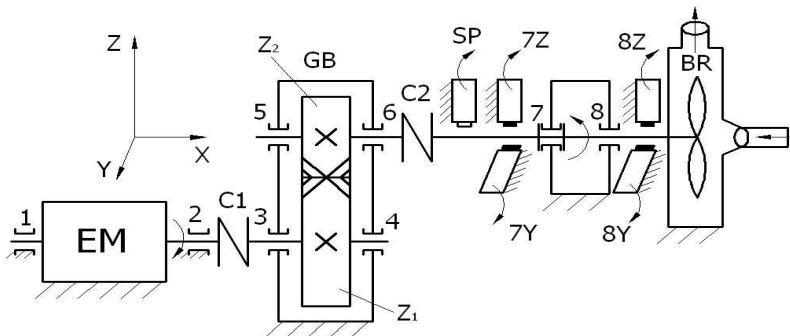

Fig. 1. The air blower machine scheme with proximity probes location: *1, 2* – journal bearings of EM; *3-6* – journal bearings of GB ($u = 0.477$, $z_2 = 43$, $z_1 = 90$); *7, 8* – tilting-pad journal bearings of BR; *C1, C2* – flexible couplings; *7Y, 7Z* and *8Y, 8Z* – proximity probes fixed at the 7th and 8th bearings, SP – keyphasor transducer
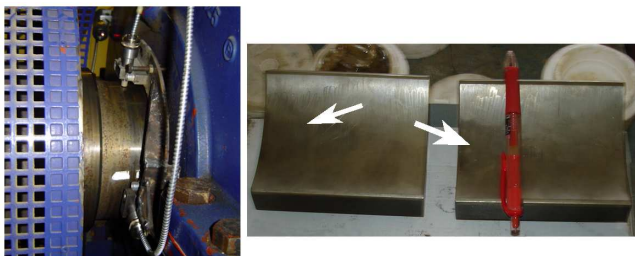

Fig. 2. The BR at 7th bearing vibration displacements peak-to-peak values s_{p-p7Z}, s_{p-p7Y} and gaps-radial clearances Δ7Y, Δ7Z measurement set with two sensors 7Z and 7Y and damaged pads

Each tilting-pad bearing comprises four pads. The failure of 7th and 8th bearings pads caused additional testing during two years continuous operation after replacement of BR new bearings. The experimental testing of the blower rotor was based on rotor vibration displacements measurement at 100%, 50% loading and at free run, coast down and run up including resonance rotational speed.

3. Vibration at varying loading

BR bearings shafts typical vibration displacement s_{p-pZ} , s_{p-pY} plots versus time and shafts kinetic orbits are presented in Fig. 3. The vibration intensity of 7th and 8th bearings is independent at different loading. The vibration displacement values of the both bearings in Y and Z directions were low and described by calculated maximum vibration displacements value s_{max} [ISO 7919-1:1996(E)]: s_{max7}=27 µm, s_{max8}=38 µm. Synchronous frequency vibration displacement amplitudes are dominated in the spectra. The vibration of 8th bearing is ~30% higher in comparison with 7th bearing - the stiffness of BR at 7th bearing is higher than at 8th bearing.
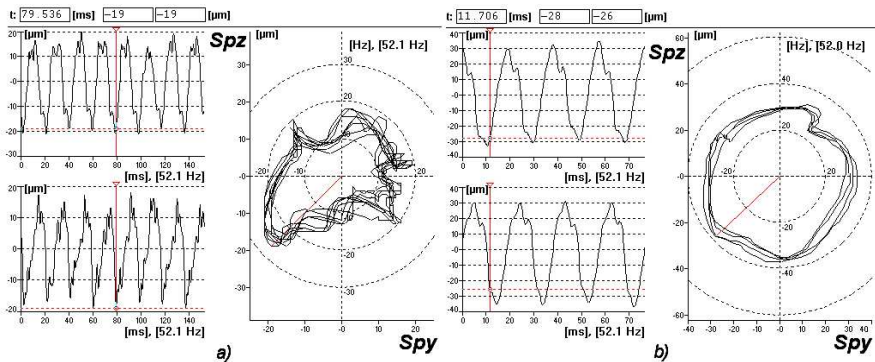

Fig. 3. BR bearings shafts typical vibration displacement s_{p-pZ} , s_{p-pY} plots versus time and shafts kinetic orbits: a) 7th bearing at 100% load, s_{max7}=27 µm; b) 8th bearing at 100% load, s_{max8}= 38 µm

4. Vibration severity at resonance

The coast down running after EM shutdown until standstill takes long length of time 841 s (Fig. 4). The run up mode from stand still till nominal rotational speed takes short length of time of 30-31 s.

After two years of continuous operation the BR dynamic stiffness decreases. The resonance frequencies decreases in comparison with new bearings case [5]. After one year of continuous operation resonance speed was 1455 rpm, but after two years - it dropped down to 1350 rpm. The maximum vibration displacements s_{max7} values of the 7th bearing became 6 times higher at the resonance (from 25 µm to 165 µm) and s_{max8} values of the 8th bearing became more than 8 times higher at the resonance (from 37 µm to 307 µm). The maximum vibration displacement peak-to-peak value s_{p-pmax} during coast down at resonance rotational speed reached 350-420 µm. At run up mode the maximum vibration displacement peak-to-peak value s_{p-pmax} at resonance reached 100-120 µm. Vibration intensity measured near resonance rotation speed at coast down and run up mode at 1914 rpm rotation speed (31.9 Hz). 7th bearing vibration displacement s_{max7}= 104 µm and for the 8th bearing - s_{max8}= 92 µm. The kinetic orbits are far from elliptical form (Fig. 5).
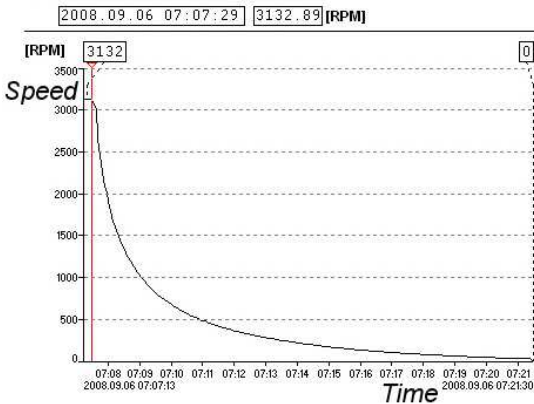
629

Fig. 4. The rotational speed timebase plot at coast down, time 841 s

Fig. 5. Maximum vibration displacements $s_{max7,8}$ values of the 7th and 8th bearings shafts versus rotational speed at coast down

The vibration severity at resonance rotation speed ~1350 rpm (22,5 Hz) reduces the clearances between the rotors and bearings. The BR provides stationary part rubbing of the tilting pad bearing elements. The vibration displacement plots and kinetic orbits are presented in Fig. 6. The BR vibration is poliharmonic with high peak amplitudes that caused rubbing at first at 8th bearing. The valuable damages was detected at the upper pad of the 7th bearing and the lower pad of the 8th bearing (Fig. 2). These damaged pads were located in vertical plane in BR.
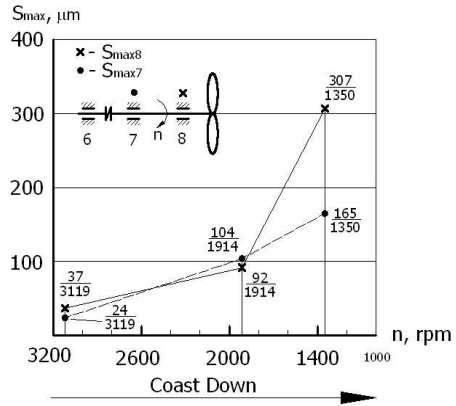

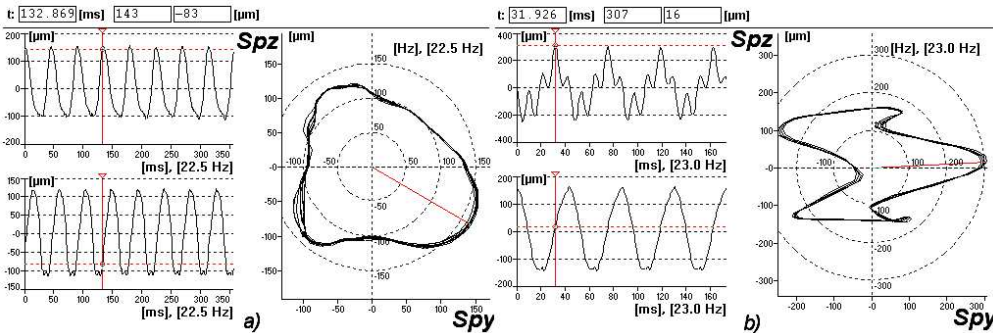**Fig. 6.** The vibration displacement plots and kinetic orbits: a) 7th bearing at resonance rotational speed, $s_{max7rez}$= 165 µm, $s_{p-pmax7Zrez}$= 250 µm, $s_{p-pmax7Yrez}$= 240 µm; b) 8th bearing at resonance rotational speed, $s_{max8rez}$=307 µm, $s_{p-pmax8Zrez}$=550 µm, $s_{p-pmax8Yrez}$=300 µm

The first reason of damaged tilting-pad journal bearings is inadmissible vibration displacement values at 8th bearing $s_{p-pmax8Zrez}$=550 µm. The vibration displacement signal at 7th bearing is lower $s_{p-pmax7Zrez}$= 250 µm, because the rotor part at 7th bearing designed with higher stiffness in comparison with free end of the rotor at 8th bearing (Fig.1). At run up the resonance phenomenon provide less vibration displacements amplitudes of the shafts in both bearings in comparison with coast down because run up time interval is comparatively short and dynamic forces have not enough time to rise up and generate valuable vibration amplitudes.

5. Shaft displacements (gaps) in the bearings

Dynamic forces that damage bearings at rubbing - contact between the rotor and stationary tilting pads - depend not only on resonance phenomenon of rotating system but on the

630

decreasing horizontal rotor gyroscopic effect when rotational speed is dropping. The rotor shaft position in the 7th and 8th bearings is described by the gaps in horizontal Y direction Δ7Y, Δ8Y and gaps in vertical Z direction Δ7Z (Fig. 7), Δ8Z. The gap value measured between tip of proximity probe and shaft cylindrical surface is described by DC signal from proximity probe output. This gap parameter evaluates gyroscopic effect of the rotor, when machine rotational speed decreases from nominal value down to standstill.
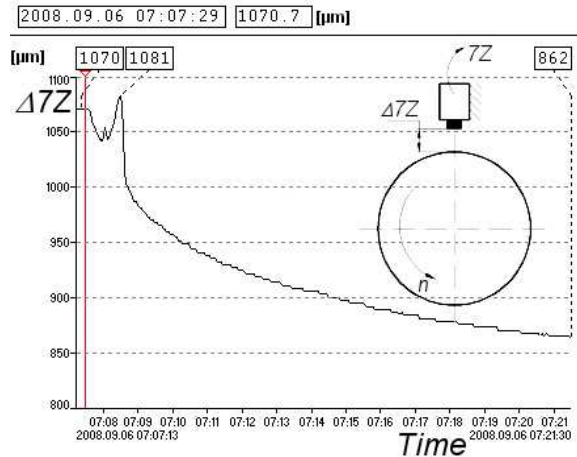

Fig. 7. The 7th bearing vertical direction gap Δ7Z plot versus time at coast down: nominal gap decreased – 208 µm at 3119 rpm; resonance gap – 219 µm at 1350 rpm and reference position 862 µm at stand still, at 0 rpm

At coast down from nominal rotational speed to standstill the blower rotor is going from the 7Y and 8Y probes located in horizontal plane (gaps increased). The gaps Δ7Y and Δ8Y are of the same order (+48 µm,…,+73 µm) and practically independent on rotational speed up to resonance (Table 1.).

Rotor displacements in vertical plane are different: the 7th bearing shaft displaced towards the 7Z probe decreasing gap by – 208 µm and the 8th bearing shaft displaced downwards increasing gap by +177 µm from the 8th probe, because gravitation force begins dominant versus gyroscopic force when rotational speed decreases below 1250 rpm value. The gap values Δ7Z and Δ8Z are displaced in opposite directions in reference to horizontal rotation axes at nominal rotational speed, but the values are slightly dependent on rotation speed up to resonance. Resonance rotational speed was reached after ~1 min at coast down.

Measured gap Δ7Y in horizontal direction at the 7th bearing changes only by 6-17 µm when rotational speed reduces from 3119 rpm to 1350 rpm. Gap Δ7Y provides valuable changes (up to 325 µm) at horizontal direction at 1200 rpm indicating increased rubbing in both bearings. The rubbing phenomenon of the rotating rotor shaft with bearing pads took part not only at 7th bearing with heavy damages of upper pad and at 8th bearing lower pad (Fig. 2.), but in all pads. The rubbing process starts at resonance speed following severe vibration displacements and substantially increased from 1250 rpm up to standstill when gravitation force of the blower rotor exceeds gyroscopic effect force.

The schematic view of rotational axes displacements in the bearings are presented in Fig. 8. The horizontal bold lines indicate rotor position at nominal speed and dashed lines - rotor position at standstill. The upper figure presents shaft axes positions in vertical *XZ* plane and lower figure – in horizontal *XY* plane, when rotation direction is counterclockwise as viewed from 7th to 8th bearing.

631

Table 1. The radial gaps between tips of proximity probes and shafts cylindrical surfaces relative to reference point

| Gap, direction	Counterclockwise direction at coast down; rotational speed of BR, rpm;			
	3132	1914	1350	Reference point
The gap value between tip of proximity probe and shaft cylindrical surface, μm (±) reference point at stand still (0 rpm)				
Δ7Y, horizontal	948-889=+59 + from 7Y probe	948-900=+48	948-883=+65	948
Δ7Z, vertical Fig. 7.	**862-1070= -208** – towards 7Z probe	**862-1050= -188**	**862-1081= -219**	**862**
Δ8Y, horizontal	845-775=+70 + from 8Y probe	845-785=+60	845-772=+73	845
Δ8Z, vertical	779-602=+177 + from 8Z probe	779-645=+134	779-607=+172	779
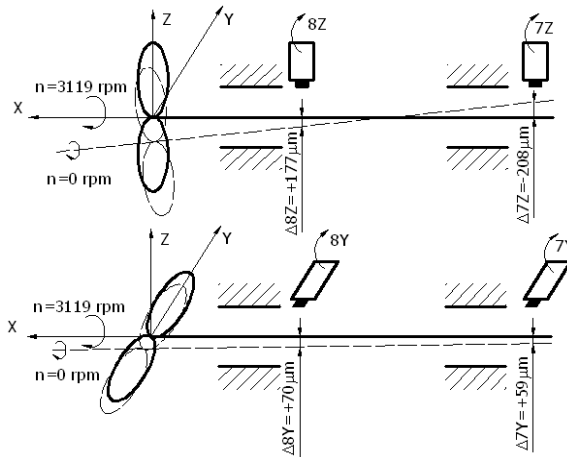
Fig. 8. The rotation axes positions of BR at nominal rotational speed and standstill

Modeling and simulation of the blower rotor is provided including gyroscopic effect of the rotor. The main task of theoretical modeling is to evaluate forces acting on journal tilting-pad bearings and to simulate shaft kinetic orbit in the bearing.

6. Mathematical modeling and simulation of air blower machine

Rotating system physical model is demonstrated in Fig. 9 (see Fig.1). All rotors are supported by tilting-pad journal bearings. The following general assumptions have been made during modeling: the materials of rotors and a coupling are elastic; shear forces are taken into account; the deflection of the rotor is described by the displacement of points of the centre line; the axial motion of the rotors is neglected.

Rotor dynamics is simulated by the finite element method when the finite element consists of two nodes and five degrees of freedom (DOF) at each node. The first and the second DOF are displacements along *Y* and *Z* axes and the last three DOF are angles around *X*, *Y* and *Z* axes. The vector of translation displacement and rotation angles of rotor finite element can be described as follows:

632

$$\left\{ \begin{array}{c} v \\ w \end{array} \right\} = \left[\begin{array}{c} N_v(\xi) \\ N_w(\xi) \end{array} \right] \{q(t)\} = [N]\{q\}, \quad \{\theta\} = \left\{ \begin{array}{c} \alpha \\ \beta \\ \gamma \end{array} \right\} = \left[\begin{array}{c} N_{1\theta}(\xi) \\ N_{2\theta}(\xi) \\ N_{3\theta}(\xi) \end{array} \right] \{q(t)\} = [N_\theta]\{q\}, \tag{1}$$

Cardin's angles are used to determine the relation between angular velocity $\{\dot{\theta}\}$ and angular velocity $\{\omega\}$ in the *XYZ* coordinate system.
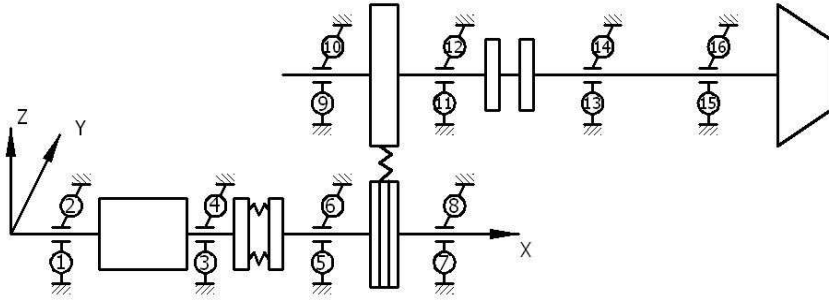

Fig. 9. Dynamic model of rotating system (see Fig.1)

To estimate dynamic regimes of EM, two-phase mathematical models are used. In the general case EM two-phase model consists of the system of differential and algebraic equations:

$$\{\dot{\psi}\} = \left[A_\psi \right]\{\psi\} + \left\{ B_\psi \left(t, \psi, \dot{\varphi}_e \right) \right\}, \tag{2}$$

$$I_e \frac{d^2\varphi_e}{dt^2} = M_e(\psi) - M_r(\varphi_i, \dot{\varphi}_i, p_{Gi}), \tag{3}$$

matrix $\left[A_\psi \right]$ and vector $\left\{ B_\psi(t, \psi, \dot{\varphi}_e) \right\}$ are equal to:

$$\left[A_\psi \right] = a_\psi \begin{bmatrix} -r_s L_r & 0 & r_s L_\mu & 0 \\ 0 & -r_s L_r & 0 & r_s L_\mu \\ r_r L_\mu & 0 & -r_r L_s & 0 \\ 0 & r_r L_\mu & 0 & -r_r L_s \end{bmatrix}, \tag{4}$$

$$\left\{ B_\psi(t, \psi, \dot{\varphi}_e) \right\} = \left\{ \begin{array}{c} \sqrt{2}U_{nom}\cos(w_s t) \\ -\sqrt{2}U_{nom}\sin(w_s t) \\ \dot{\varphi}_e \psi_4 \\ -\dot{\varphi}_e \psi_3 \end{array} \right\}, \tag{5}$$

torque of EM is equal to:

$$M_e = \frac{3}{2} \cdot pol \cdot L_\mu a_\psi (\psi_1\psi_4 - \psi_2\psi_3), \tag{6}$$

$$a_\psi = 1/L_s L_r - L_\mu^2. \tag{7}$$

633

The equations of motion of the rotor finite element are derived by applying Lagrange equation of the second order and can be written as follows:

$$[M(q)]\{\ddot{q}\} + ([C] + [G])\{\dot{q}\} + [K]\{q\} = \{F(q, \dot{q}, \psi)\},$$ (8)

7. Tilting-pad journal bearing model

Under the assumption of small displacements of the journal centre, the fluid-film force components in the horizontal and vertical directions, F_{by} and F_{bz}, are as follows:

$$\{F_b\} = \begin{Bmatrix} F_{by} \\ F_{bz} \end{Bmatrix} = \{F_b(v, w, \dot{v}, \dot{w},)\},$$ (9)

where k_{ij} and the c_{ij} $(i, j) = (y, z)$ are stiffness and damping coefficients respectively.

The stiffness and damping matrix of tilting-pad journal bearing are equal to:

$$[K_b] = \left[\frac{\partial\{F_b\}}{\partial\{q_b\}} \right], \ [C_b] = \left[\frac{\partial\{F_b\}}{\partial\{\dot{q}_b\}} \right]$$ (10)

$\{q_b\}^T = [v_b, w_b]$ vector of bearing displacement.

The hodograph of the relative hydrodynamic force $(F_{br}/F_{br\,max})$ in the radial direction of tilting-pad journal bearing is presented (Fig. 10).
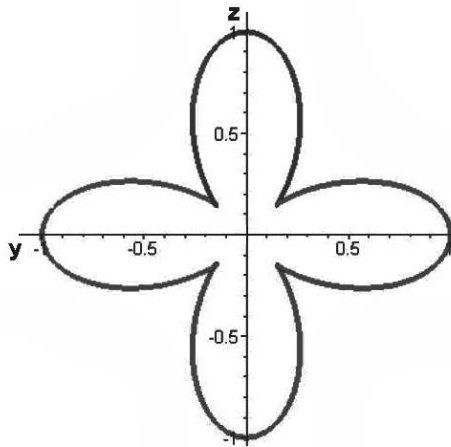

Fig. 10. The hodograph of relation tilting-pad journal bearing forces

8. Simulation results

Simulation results are presented in shafts kinetic orbits format in Fig. 11 at nominal rotational speed and were verified by experimental measurements (Fig. 3).
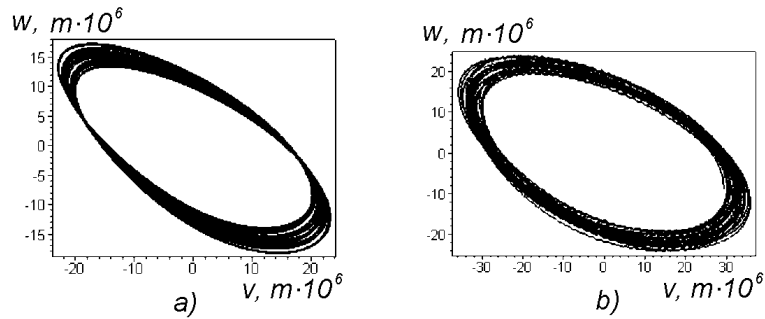
634

Fig. 11. Simulated kinetic orbits of 7th (a) and 8th (b) bearings shafts at nominal rotational speed 3132 rpm: W – Z axes, V– Y axes

Simulated results indicate that rotor vibration is dependent on unbalance, variable dynamic stiffness and on impeller gyroscopic effect. In case of rotor center of mass shift fro geometrical axis in 0.02 mm, when mass of the rotor is 2900 kg, rotational speed 3120 rpm, inertia force is 6190 N. Gyroscopic moment of the rotor have the same influence. Nominal rotational speed of the rotor is more than twice higher than its resonance frequency as experimentally measured ~22.5 Hz. The transient rotation running processes of BR acceleration and deceleration should be performed as fast as possible to pass resonance frequency and as short as possible after resonance rotational speed in coast down mode.

9. Conclusions

The coast down mode is the most dangerous running mode for the blower rotor tilting-pad journals bearings because it causes rub phenomenon of the rotating rotor shafts with bearings pads.

The rubbing process starts first at 8th bearing at resonance rotational speed of 1350 rpm because of inadmissible vibration displacement amplitude maximum value $s_{max8} = 307$ µm.

The gyroscopic effect of the BR wheel changes shafts positions described by gaps in the 7th and 8th bearings increasing rubbing process at 1250 rpm till stoppage of the rotor and it takes long length of time 13 min. Experimental measurements indicated that 7th bearing shaft goes up (in vertical direction) 208 µm and 8th shaft displaced down 177 µm during the coast down mode.

Experimental testing results verified theoretical modeling and simulation results.

References:

[1] **Barzdaitis V., Bogdevičius M., Gečys St.** Vibration problems of high power air blower machine.-2nd International Symposium on Stability Control of Rotating Machinery, ISCORMA-2. Proceedings. - Gdansk, Poland; Minden, Nevada, USA, 2003, p.606-616.

[2] **Bently D. E.** Fundamentals of Rotating Machinery Diagnostics. Library of Congress Control Number 2002094136, Bently Pressurized Bearing Company, printed in Canada, 2002.-726p.

[3] **Aladjev V., Bogdevičius M.** Maple 6: Solution of the Mathematical, Statistical and Engineering – Physical Problems. Moscow: Laboratory of Basic Knowledge's, (2001) p.824 (in Russian).

[4] **Goldin A. S.** Vibration of Rotating Machines, ISBN 5-217-02927-7, UDK 621.752, BBK 22.23 G63.- Moscow: Mashinostroenie, 2000.-344p. (in Russian).

[5] **Vasylius M., Didžiokas R., Mažeika P., Barzdaitis V.** The rotating system vibration and diagnostics. – Mechanika. – Kaunas, Lithuania: Technologija, 2008, Nr. 4(72), p. 54-58.

[6] **Khonsari M. M., Chang Y. J.** Stability boundary of non-linear orbits within clearance circle of journal bearings, ASME Journal of Vibration and Acoustics, 115

635